EEF1A2 D91N geometry in a modeled complex with EEF1B2 and GDP

Filippo D. Galbo
Independent researcher
Corresponding author: fgalbo@outlook.com

24 November 2026

Abstract

Asp91 lies near the GDP-binding site of human eukaryotic elongation factor 1A2 (EEF1A2). We asked how the neurodevelopmental variant D91N changes the positions of GDP and the exchange factor EEF1B2 in a modeled complex. We examined six structural predictions, three exploratory Mg-containing trajectories and nine 25 ns Mg-free trajectories built from one wild-type (WT) scaffold. D252H served as a secondary comparator. During minimization, the shortest residue-91–GDP heavy-atom distance increased from 4.81 to 5.75 Å in WT and changed from 4.85 to 4.84 Å in D91N. The same GDP β-phosphate oxygen was closest in both conditions. All three D91N trajectories began production with shorter distances than all three WT trajectories. Over 5–25 ns, the means were 5.4 and 7.5 Å, respectively. Core and EEF1B2 fragment deviations overlapped at production zero and separated over different averaging windows. Two D91N trajectories retained trans Asn91 and sampled an Asn91–water–GDP bridge in 97 and 122 of 201 frames. The third changed rotamer before 0.6 ns and had no bridges in that window. No direct residue-91 side-chain hydrogen bond to GDP met the geometric criteria. These results locate the distance difference during preparation of this scaffold. Whether D91N alters basal or EEF1B2-stimulated GDP release requires kinetic measurements at matched concentrations of active protein.

Introduction

EEF1A2 delivers aminoacyl-tRNA during translation. Its exchange factor accelerates GDP release, permitting GTP to bind for the next elongation cycle. Comparing rabbit GDP-bound EEF1A2 with yeast exchange-factor complexes, Crépin and colleagues described Asp91 turning toward the nucleotide site, where it can form a salt bridge with Lys20 and a hydrogen bond with Ser21 [1,2,10]. Biochemical experiments in yeast also implicate exchange-factor Lys205 in nucleotide exchange [3]. Its human EEF1B2 counterpart is Lys224. D91N replaces an anionic carboxylate with a neutral amide of comparable size, allowing us to ask which features of this local geometry depend on the residue at position 91.

Human sequencing studies have reported EEF1A2 p.Asp91Asn in the setting of neurodevelopmental disease [4]. Paulet and colleagues also reported a mosaic D91N case with a milder presentation than previously described cases [12]. Carvill and colleagues found reduced steady-state abundance for yeast Tef2 D91N and observed that it failed to restore growth in plasmid-shuffle and rapamycin-challenge assays [13]. A separate study expressed the analogous substitution in V5-tagged yeast Tef2. D91N was among eight of nine variants with lower steady-state protein levels than WT in wild-type yeast [5]. D91N turnover was not measured in that experiment. The authors observed accelerated turnover for F98C in a separate comparison. These results make the abundance of functional protein an important alternative explanation to examine alongside exchange kinetics in human EEF1A2.

We compared D91N with WT to determine whether the mutation was associated with reproducible differences in the positions of GDP or EEF1B2 under one modeled preparation. We included D252H as a

secondary comparator. Davies and colleagues found impaired recovery of eEF1B with D252H EEF1A2 by co-immunoprecipitation in transfected SH-SY5Y cells [6]. This cellular association phenotype motivates the comparator but supplies no quantitative calibration for a single atom-pair distance in a binary complex.

Methods

Structural inputs and earlier cohorts

We examined rabbit GDP/Mg-bound EEF1A2 (4C0S [1]), nucleotide-free yeast eEF1A–eEF1Bα (1F60 [10]) and the yeast complexes deposited as 1G7C, 1IJE and 1IJF [2]. Boltz-2 v2.2.1 [7] generated full-length human EEF1A2–EEF1B2 predictions with GDP and Mg for WT, D91N and D252H, with one diffusion sample at each of two prediction seeds (11 and 23). Distances selected in the first seed were remeasured in the second. We compared homolog identities, order and pairing keys across sequence alignments. WT seed 11 used the original alignment. The other five predictions used normalized alignments.

An initial molecular-dynamics pilot used the three condition-specific seed-11 predictions with full-length EEF1B2 and Mg. Each condition had a single 10 ns production trajectory. A retrospective audit examined 3,000 saved full-system frames and 15,000 scalar samples across these three trajectories. Their distinct starting poses, chemistry and nonbonded settings precluded pooling them with the redesigned comparison. Technical capacity and qualification runs were excluded from both production cohorts.

Molecular dynamics from a common scaffold

The nine Mg-free systems shared the backbone of the WT seed-23 prediction. Each contained EEF1A2 residues 1–463, an N-acetyl-capped EEF1B2 fragment spanning residues 112–225, and GDP. The fragment retained all 110 interprotein residue pairs within 5 Å in at least five of the six static models. EEF1B2 residues 112–133 extended beyond the homologous experimentally modeled fragment. To build D91N, the N, Cα and C atoms of the seed-23 donor Asn91 were aligned to WT residue 91. The donor contributed CB, CG, OD1 and ND2. A separate WT preparation with Mg failed its coordination check when the Mg–GDP O2B distance shortened from 2.1 to 1.8 Å, below the specified 1.9–2.6 Å interval. Histidine states were fixed following a pH 7 assessment, with EEF1A2 His95 protonated at NE2 and comparator His252 provisionally protonated at ND1. Each condition had one prepared solvent box.

OpenMM 8.4.0 [8] simulations used CUDA mixed precision, the installed CHARMM36 2024 parameters, CHARMM TIP3P water, 0.15 M added NaCl and neutralizing ions. A rhombic dodecahedral box provided 1.0 nm padding. Particle mesh Ewald electrostatics used a 1.2 nm cutoff. Lennard-Jones forces switched from 1.0 to 1.2 nm. LangevinMiddle dynamics used 300 K, friction of 1 ps^{-1} and a 4 fs time step, with nonwater solute hydrogen masses repartitioned to 3.0 amu. Water was rigid, bonds involving hydrogen were constrained, and a Monte Carlo barostat targeted 1 bar. Each seed underwent its own minimization and 600 ps of equilibration. The first 100 ps used NVT at a heavy-solute restraint of 1000 kJ mol^{-1} nm^{-2}. NPT followed for 200, 200 and 100 ps at 1000, 100 and 0 kJ mol^{-1} nm^{-2}, respectively. The three minimized solute structures in each condition coincided at saved precision. Each seed had a distinct equilibrated structure. Three runs per condition used random seeds 11, 23 and 47 for velocity initialization, thermostat and barostat randomness. Each produced 25 ns of unrestrained dynamics. Production zero followed minimization and the nominal 600 ps staged equilibration protocol; the protocol label does not establish physical equilibration. Elapsed production time in ns was production_step × 0.000004, rather than the stored time_ps clock that includes equilibration. Scalar measurements were sampled every 2 ps, solute coordinates every 10 ps and full-system coordinates every 100 ps.

Endpoints, replication and acceptance

Before production, the analysis specified six primary, twelve secondary and two legacy endpoints. Table 1 lists all six primary measurements. For partner RMSD, an unweighted proper rigid Kabsch fit aligned the same 120 prespecified EEF1A2 Cα atoms to the corresponding source shared-backbone structure before protonation, minimization and equilibration. The fit was applied once to EEF1B2 and GDP, without a second partner or ligand fit. These RMSDs measure deviation from the pre-preparation reference and do not isolate motion acquired during production. Companion measurements used EEF1B2 residues 136–225 or restricted site-91 distances to terminal polar atoms. The secondary residue-91–GDP endpoint minimized the distance between source-structure heavy atoms of residue 91, including backbone and side chain, and source-structure GDP heavy atoms. All primary analyses used the inclusive 5–25 ns interval, with 10,001 correlated scalar observations per run. We report arithmetic means and sample standard deviations across three trajectory means per condition. The trajectories are conditional replicates under one construction and solvation setup per condition, without independent preparation replication. Matching numerical seed labels support descriptive comparisons and do not create physically paired experiments. Frames and time blocks are not independent replicates; all contrasts and spread comparisons are descriptive, without formal significance or equivalence claims.

Distance endpoints used the nearest of 27 periodic images around the fractionally nearest cell in the reduced triclinic box. Lys224 NZ-to-GDP distance minimized over GDP O1B, O2B and O3B. The all-side-chain residue-91 endpoint included CB and CG; its terminal-only companion used Asp91 OD1/OD2 or Asn91 OD1/ND2. The legacy A91 O–B224 N distance used backbone atoms. For RMSD, molecules were reconstructed using topology bonds and a single whole-molecule lattice translation chosen to preserve the original relative placement. GDP RMSD used 28 source heavy atoms with identity correspondence and no equivalent-oxygen permutation. The file data/definitions/endpoint_specification.json records the atom selections for all 20 endpoints.

The first WT run (seed 11) completed 25 ns but failed its original constraint-residual screen. After inspecting this run, the acceptance policy was revised. Hard limits included finite sampled values, maximum relative constraint residual $\leq 10^{-4}$, mean production temperature within 2 K of 300 K and maximum core-fitted GDP RMSD ≤5 Å. The integrator tolerance stayed at 10^{-5}. In WT11, 63 of 12,500 positive-time production samples exceeded 10^{-5}, with a maximum of 1.46×10^{-5} in production. All nine runs passed the revised numerical screens. The production records contain sampled relative constraint residuals above 10^{-5} in all nine runs, with 33–67 such samples per run and none above 10^{-4}. WT11 was the first run assessed under the original policy, not the only run with such exceedances. We also calculated the fragment RMSD contrast excluding only WT11 as a post hoc sensitivity check. These checks address numerical acceptance, while physical equilibration remains a separate question. Exclusion sensitivity does not establish that WT11 geometry is a numerical artifact.

Post hoc analysis of the saved coordinates

We examined every 10 ps solute frame and every 100 ps full-system frame in the 5–25 ns window (2,001 and 201 frames per run, respectively). We inspected the preceding production interval separately to locate observed residue-91 rotamer-class changes. Dihedrals used N–Cα–Cβ–Cγ for χ1 and Cα–Cβ–Cγ–OD1 for χ2. The χ1 classes were gauche-minus from −120° to <0°, gauche-plus from 0° to <120°, and trans otherwise. For comparisons of Asp side-chain orientation, chemically equivalent terminal oxygens motivate a χ2 period of 180°. Asn χ2 retains the distinction between OD1 and ND2 and was analyzed with a 360° period.

We identified hydrogen-bond geometry from the prepared topology and explicit hydrogens using a donor–acceptor distance ≤3.5 Å and donor–H–acceptor angle ≥150°. A one-water bridge required the same water molecule to meet both hydrogen-bond criteria within one full-system frame. Its occupancy

counts frames with at least one qualifying water. We separately screened direct interactions of the residue-91 terminal groups with protein and GDP atoms in the solute frames. Occupancies describe saved snapshots. The 100 ps sampling does not resolve continuous water residence times.

Using the original EEF1A2 core fit and whole-molecule periodic imaging, we partitioned the 114-residue partner mean squared deviation from the fixed pre-preparation reference into contributions from B112–135 (24/114 weight) and B136–225 (90/114). For each Cα atom, root-mean-square fluctuation (RMSF) was calculated around its own run-mean position after that same fit. These fluctuations retain partner motion relative to EEF1A2 and are not a partner-internal flexibility measurement. Weighted segment mean squared reference deviations add; time-averaged RMSDs do not. We compared the reconstructed whole-fragment, shorter-fragment and EEF1A2 core RMSDs with the archived scalars at all 22,509 stored solute timestamps over 0–25 ns.

Preparation-stage geometry, the early scalar windows and the expanded crystal comparison were post hoc, added 23 November 2026. We used the nine original production scalar files and the saved structures and stage-specific scalar records. For each of 20 endpoints we recorded the single step-zero value, means over [0, 0.1), [0, 1) and [4, 5) ns, and the inclusive 5–25 ns mean. Sensitivity windows included both endpoints at 0–25 and 12.5–25 ns. Complete separation required all three variant run estimates to lie on the same side of all three WT estimates. We also compared the absolute condition-mean difference with the larger within-condition range of the three run means. These are distinct descriptive criteria. The supplementary CSVs retain the archived values to 0.001 Å or finer precision.

On 24 November 2026 we froze the rules for a post hoc audit of the atom pair furnishing the residue-91–GDP minimum. At each of 37 saved preparation checkpoints we ranked all 224 combinations of eight residue-91 heavy atoms and 28 GDP heavy atoms using Cartesian distances for unsolvated coordinates and minimum-image distances when the saved system included a periodic cell. We retained source atom names and treated distances within 0.001 Å of the minimum as tied. The audit distinguishes the identity of the closest pair from changes in its distance.

We measured the first deposited coordinate model of each reference. For alternate sites we selected the residue conformer with the highest mean positive occupancy, retained its shared atoms and resolved ties by altloc identifier. We measured Cartesian distances within each asymmetric-unit copy using observed atoms. The sequence alignment of yeast EFB1 (P32471) and human EEF1B2 (P24534) maps yeast Lys205, deposited as B1205, to human Lys224. Rabbit 4C0S chains A and B were analyzed separately. We compared homologous backbone and side-chain contacts independently, without symmetry mates, fitted structures or reconstructed phosphate atoms.

Results

Predictions and the pilot containing magnesium

In the static D91N models, the EEF1A2 Lys20–site91 Cα distances exceeded WT by 0.8 and 0.3 Å at prediction seeds 11 and 23. The backbone O91–EEF1B2 N224 contrasts were +1.2 and −0.4 Å. In the seed-11 models, the nearest site-91 heavy atom lay 6.1 Å from GDP in D91N and 4.8 Å in WT. For D252H minus WT the Cα contrasts were −0.3 and −0.2 Å, and the backbone contrasts were both positive (less than 0.1 Å at seed 11 and 0.1 Å at seed 23). Sequence deduplication at the alignment-size cap could replace one of 8,191 retained homologs following a query substitution. Removing the same six query-colliding records across conditions produced identical retained homolog sets. The structural effect of this correction was unmeasured.

The three Mg-containing pilot runs reached different coordination geometries. At 10 ns, five oxygen atoms lay within 2.5 Å of Mg in WT, including Asp91 OD2. Six lay within that distance in D91N, including Ser21 OG and three GDP oxygens. The D252H terminal shell likewise contained six oxygens but

comprised two GDP oxygens and four waters. Both the starting pose and the solvent/coordination environment varied across these runs. The reference structures also incompletely resolved the local Mg or nucleotide environment. These observations motivated the common scaffold and explicit chemical-state choice used for the replicated comparison.

D91N in the replicated panel with GDP

Table 1. Prespecified primary endpoints for the nine 25 ns trajectories. Each entry gives the mean ± sample standard deviation of three run means over 5–25 ns. A indicates EEF1A2 and B indicates EEF1B2. NZ denotes the terminal lysine nitrogen. Percentage standard deviations are in percentage points. Distance minima were evaluated at each sampled time before averaging.

Measurement	WT	D91N	D252H comparator
A252 side-chain to B Lys147 NZ, Å	2.72 ± 0.01	2.72 ± 0.02	3.72 ± 0.98
A252–B Lys147 occupancy below 3.5 Å, %	99.99 ± 0.01	99.98 ± 0.03	59.39 ± 52.42
B Lys224 NZ to nearest GDP β-phosphate oxygen, Å	7.94 ± 0.26	7.71 ± 0.20	8.42 ± 0.14
B Lys224 NZ to nearest A91 side-chain heavy atom, Å	8.61 ± 0.05	7.74 ± 0.65	8.86 ± 0.15
B112–225 Cα RMSD after fit on EEF1A2, Å	2.17 ± 0.16	2.62 ± 0.22	2.33 ± 0.70
A/B protein heavy-atom pairs below 4.5 Å	509.37 ± 36.49	549.03 ± 58.41	546.05 ± 36.80

The primary Lys224 NZ–residue-91 side-chain minimum was shorter in D91N than WT by 1.1, 1.3 and 0.2 Å at matching seed labels. For the terminal polar atoms alone the differences were −2.4, −2.4 and +0.3 Å. The residue-91–GDP minimum across all source heavy atoms (S09) averaged 5.4 ± 1.3 Å for D91N and 7.5 ± 0.2 Å for WT over 5–25 ns. The D91N run means were 4.8, 4.6 and 6.9 Å, and the WT means were 7.8, 7.4 and 7.4 Å. At production zero, D91N values were already shorter in all three runs (5.2, 4.7 and 4.7 Å versus 7.8, 6.4 and 6.6 Å for WT, Figure 1). Other pocket residues differed in direction. At residues 95, 101 and 107 the mean D91N minus WT differences were +0.1, −0.2 and −1.7 Å, with a WT between-run SD of 2.9 Å at residue 107.

Construction and solvation gave nearly equal residue-91–GDP minima in WT (4.81 Å) and D91N (4.85 Å). At minimization the WT minimum increased to 5.75 Å, while the D91N minimum changed to 4.84 Å (Figure 1). In WT, Asp91 OD2 was initially closest to GDP O2B. Its distance increased from 4.81 to 6.10 Å, and the other carboxylate oxygen, OD1, became closest. In D91N the Asn91 ND2–O2B pair remained closest through minimization. At each of the 37 checkpoints, the next closest pair lay more than 0.001 Å above the minimum. At production zero, OD1–O2B was closest in all three WT and all three D91N runs. During equilibration, 296 of 300 sampled time points placed all three D91N values below all three WT values. Their ranges overlapped at 72, 380, 486 and 492 ps. By the end of equilibration the D91N mean was 2.1 Å below WT.

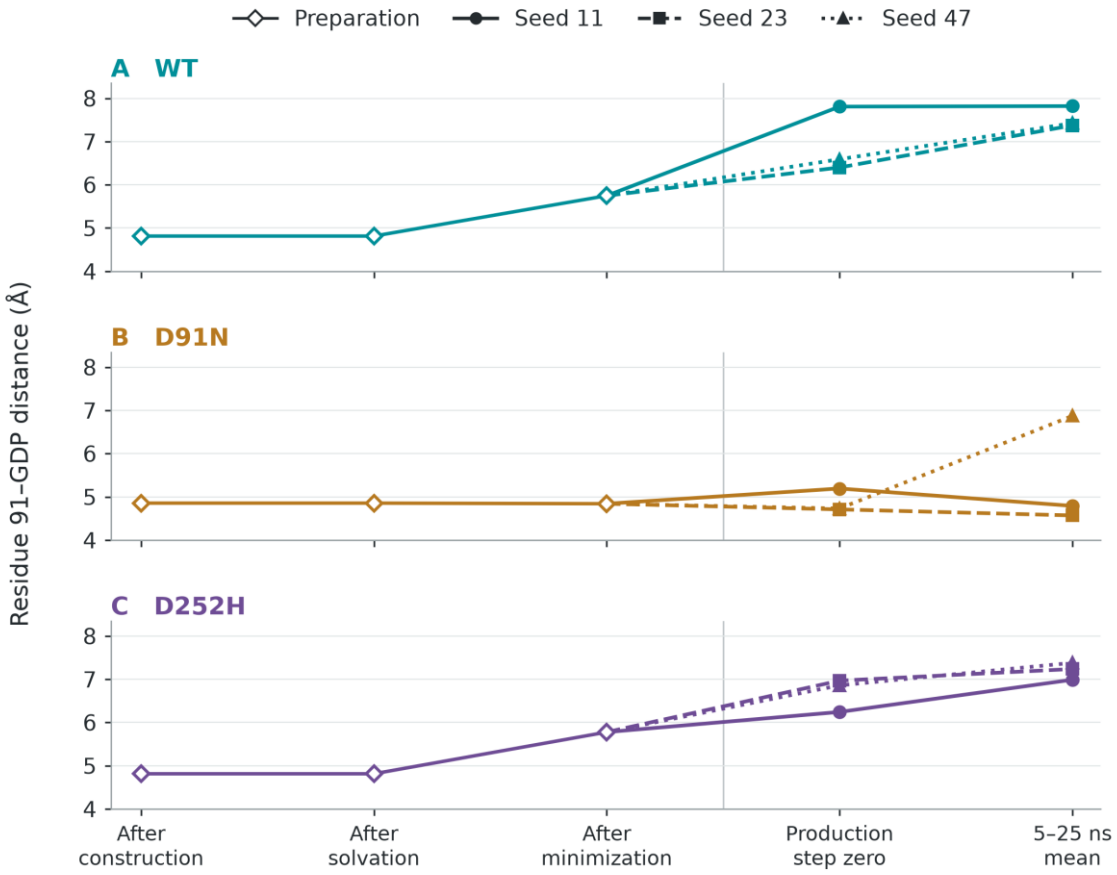


Figure 1. Minimum residue-91–GDP heavy-atom distance in WT (A), D91N (B) and D252H (C). Open diamonds show the construction, solvation and minimization checkpoints. Each minimized value represents three jobs with identical saved solute coordinates at the reported precision. Filled symbols identify individual seeds at production zero and their mean distances over 5–25 ns. Lines connect saved summaries. Horizontal spacing denotes stages, with 600 ps of staged equilibration between minimization and production zero.

When the core and partner deviations separated

At production zero, the D91N and WT ranges overlapped for both RMSDs. The core first-nanosecond means separated, although the ranges overlapped again for the 4–5 ns window. The fragment started lower on average in D91N, showed overlap through the 4–5 ns averages, and separated in the 5–25 ns averages. Production zero is a single frame and the subsequent values are window means. The observations do not date the first instantaneous crossing. Table 2 gives the contrasts, and Supplementary Figure S4 shows the running means.

Table 2. D91N minus WT differences between condition means. An asterisk indicates that all three estimates in one condition lie on the same side of all three in the other. Displaying three decimal places distinguishes the early contrasts. The primary window includes both endpoints.

Production window (ns)	Residue 91–GDP (Å)	Core RMSD (Å)	B112–225 RMSD (Å)
Step 0	−2.056 *	+0.086	−0.195
0–<0.1	−2.517 *	+0.245	−0.113
0–<1	−2.214 *	+0.321 *	−0.055
4–<5	−2.309 *	+0.263	+0.015
5–25	−2.128 *	+0.227 *	+0.452 *

At seeds 11, 23 and 47, the fragment RMSD over 5–25 ns was 2.5, 2.5 and 2.9 Å for D91N and 2.2, 2.0 and 2.3 Å for WT. The difference between condition means exceeded the range within either condition in this window. Across 0–25 ns the difference was 0.4 Å and the larger within-condition range was 0.5 Å. Excluding WT11 gave a primary-window difference of +0.5 Å (three D91N and two WT runs). Restricting the calculation to residues B136–225 gave D91N minus WT differences of −0.2, +0.2 and +1.2 Å by seed. D91N47 averaged 3.4 Å for this segment in the first analyzed 10 ns and 2.6 Å in the second.

For core RMSD the difference between condition means exceeded the larger within-condition range in each of the three sensitivity comparisons (0–25, 5–25 and 12.5–25 ns). For fragment RMSD, the full-window difference exceeded the larger between-run SD, but fell within the larger range. The data package reports both criteria for every window in data/tables/scalar/spread_and_separation.csv.

Interprotein heavy-atom pair counts differed in direction across seed comparisons. The D252H site252–Lys147 contact occurred in 78.85%, 0.03% and 99.30% of sampled times at seeds 11, 23 and 47. In 251 full-system frames per trajectory over 0–25 ns, sodium lay within 3.0 Å of a GDP β oxygen in 185, 128 and zero D91N frames (73.7%, 51.0% and 0%). These snapshot counts do not resolve ion residence times or establish that sodium substitutes for Mg.

Lys224 geometry and structural references

Over 5–25 ns the mean Lys224 NZ–GDP β-oxygen distances were 7.9 ± 0.3 Å for WT, 7.7 ± 0.2 Å for D91N and 8.4 ± 0.1 Å for D252H. Corresponding NZ–Ser21 OG distances were 7.6 ± 0.5, 7.4 ± 0.5 and 8.3 ± 0.8 Å. The sampled minima across the nine trajectories in this window were 5.7 Å to GDP β oxygen and 5.3 Å to Ser21 OG. WT23 reached 5.2 Å to Ser21 over 0–25 ns. In yeast the equivalent NZ–Ser21 OG distance was 2.8 Å in nucleotide-free 1F60 [10] and 2.9, 2.8 and 2.9 Å in 1G7C, 1IJE and 1IJF [2], respectively (Figure 2). None of these four entries contained observed GDP β-oxygen coordinates. The GDPNP-condition structure 1G7C contains the monophosphate component 5GP.

Table 3. Geometry in deposited structures and primary-window human run means. Yeast ranges span four entries [2,10]. Rabbit 4C0S values correspond to chains A and B, respectively [1]. The human model column uses three WT runs for the two docking contacts and nine runs for loop spacing and terminal lysine position. Human residue numbers identify the homologous pairs.

Measurement	Yeast complex	Rabbit 4C0S	Human model
A252 side chain–B147 NZ (Å)	2.70–2.80	No partner	2.71–2.73
A91 O–B224 N (Å)	2.81–2.89	No partner	2.90–2.98
A20 Cα–A91 Cα (Å)	7.29–7.40	10.86, 10.60	7.17–8.13
B224 NZ–A21 OG (Å)	2.78–2.94	No partner	6.86–9.24
Residue-91 χ1 class	trans (4/4)	trans, trans	WT gauche-minus in 5–25 ns

WT reproduced the yeast A252–B147 side-chain distance. Its A91 O–B224 N run means lay just above the yeast range (Table 3). Across all nine human models the A20–A91 Cα run means were nearer the yeast distances than either copy of rabbit 4C0S. All four yeast Asp91 side chains and both rabbit copies were trans. The counterpart of human A252 is yeast A250, and the two exchange-factor lysines B147 and B224 correspond to yeast author residues B1128 and B1205.

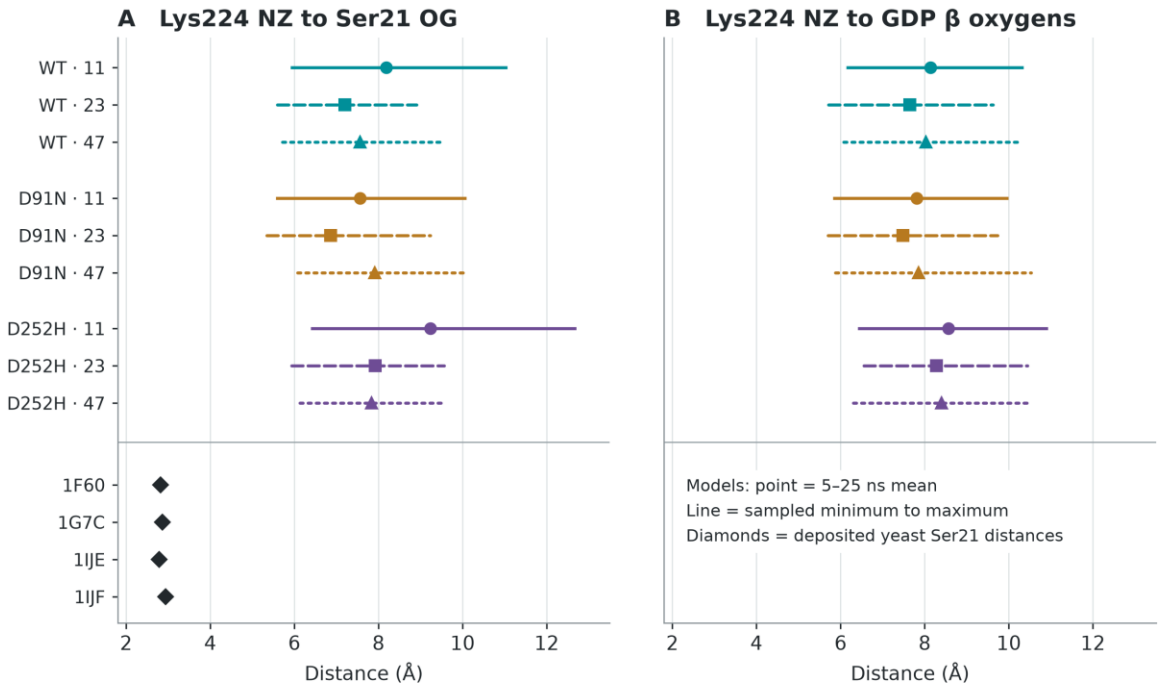


Figure 2. EEF1B2 Lys224 NZ to EEF1A2 Ser21 OG and to the nearest GDP β oxygen in each human-model trajectory. Markers and lines give 5–25 ns means and sampled ranges. Yeast Lys205 NZ–Ser21 OG values are direct asymmetric-unit distances in 1F60 [10], 1G7C, 1IJE and 1IJF [2]. No β oxygen was modeled in these yeast entries. The alternative refinement 5O8W uses the diffraction data from 1F60 [10,11].

Coordinate evidence for distinct residue 91 geometries

Asn91 was trans in the unminimized D91N input and at production zero in all three runs. D91N11 and D91N23 retained trans throughout sampled production. D91N47 changed from trans to gauche-minus between 0.58 and 0.59 ns at 10 ps sampling, with no observed return to trans. Its distance to GDP still occasionally fell below the exploratory 5.5 Å threshold (0.81% of primary-window scalar samples). Each D91N run occupied its respective rotamer in all 2,001 primary-window solute frames. WT11 entered production gauche-minus, and WT23 and WT47 entered trans. All three WT runs were gauche-minus throughout 5–25 ns. Circular-mean D91N χ1 angles were −172°, −179° and −65° in seed order. Corresponding OD1-defined χ2 means were +16°, +13° and +110°.

Asn91 terminal polar atoms supplied the nearest side-chain atom to B Lys224 NZ in 99.30%, 99.65% and 0% of solute frames. ND2 and GDP O2B were the nearest residue-91/GDP heavy-atom pair in 78.51%, 74.91% and 92.10%. A one-water hydrogen-bond connection between the Asn91 terminal group and GDP O2B occurred in 97/201 (48.3%), 122/201 (60.7%) and 0/201 sampled full-system frames. WT and D252H each had zero qualifying bridges across their three runs. No direct hydrogen bond from the residue-91 terminal groups to GDP or to B Lys224 NZ met the criteria. We also found no one-water bridge to that NZ. The Lys224 backbone gave a different result. Asn91 ND2 donated to the B Lys224 backbone carbonyl oxygen in 205/2,001 and 42/2,001 solute frames at seeds 11 and 23. It donated to EEF1A2 Ser21 OG in 494/2,001 and 567/2,001 frames, respectively. At seed 47, Thr24 OG1 formed a hydrogen bond with Asn91 in 1,028/2,001 frames, accepting from ND2 in 987 and donating to OD1 in 41. WT Thr24 OG1 donated a hydrogen bond to the Asp91 carboxylate in 1,722, 1,916 and 1,952 of 2,001 solute frames at seeds 11, 23 and 47. Figure 3A shows the bridge counts.

In an exploratory check of the initial interval in D91N seed 47, a water linked Asn91 to GDP in five of six full-system frames from 0.0 through 0.5 ns. The bridge was absent at 0.5 ns and at every subsequent full-system sample (0/44 at 0.6–<5 ns and 0/201 at 5–25 ns). Before and after the observed rotamer change, respectively, Asn91 formed a hydrogen bond with Ser21 in 24/59 and 0/441 solute frames, and with Thr24 in 0/59 and 76/441. These solute counts cover 0.00–0.58 ns and 0.59–<5 ns. These early windows were selected after inspection. The 100 ps spacing of the water frames precludes ordering individual water and torsional events or establishing that one caused the other.

Hydration and contributions of the partner segments

The reconstructed core and two partner RMSDs agreed with their runtime values to within 4.5×10^{-7} Å at matched timestamps. At 10 ps coordinate sampling, the D91N minus WT difference in whole-fragment mean squared reference deviation was +2.303 Å^2. After weighting by residue count, B112–135 contributed +0.750 Å^2 and B136–225 contributed +1.553 Å^2. The two contributions were +2.096 and −0.510 Å^2 at seed 11, +1.659 and +0.559 Å^2 at seed 23, and −1.506 and +4.611 Å^2 at seed 47 (Figure 3B). For the same segments the differences in mean per-residue RMSF were +1.7, +0.7 and −0.4 Å for B112–135 and +0.3, +0.1 and less than +0.1 Å for B136–225.

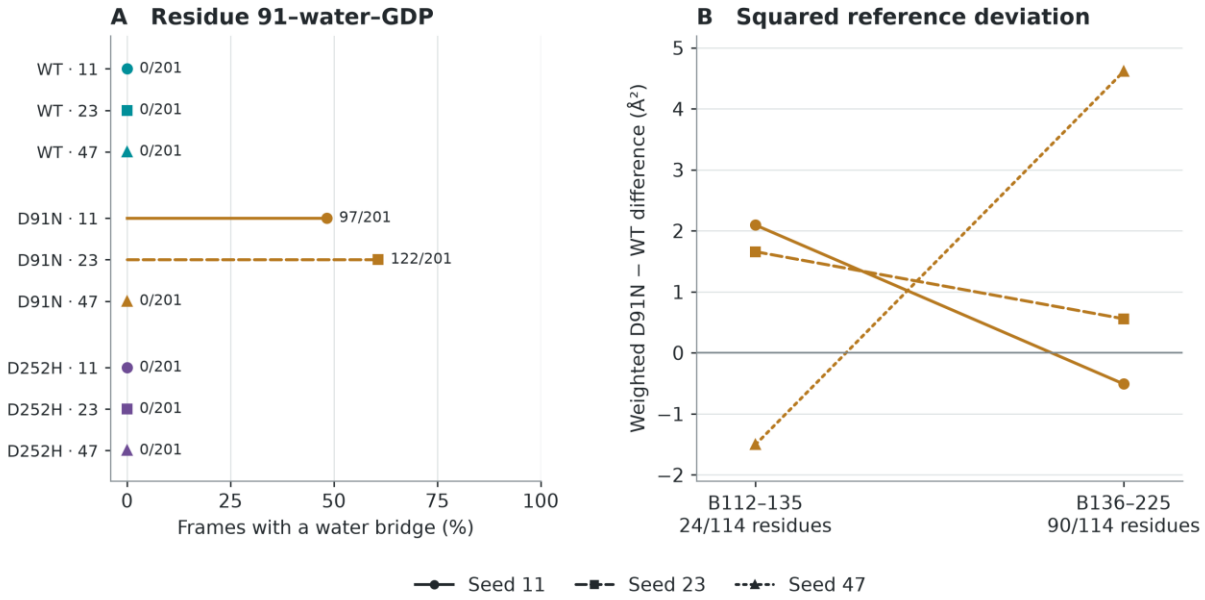


Figure 3. A, Full-system frames with a residue-91 terminal-group–water–GDP O2B hydrogen-bond bridge in 5–25 ns, out of 201 per trajectory. The terminal atoms belong to Asn in D91N and Asp in WT and D252H. All six WT and D252H runs had zero qualifying frames. B, Residue-count-weighted B112–135 and B136–225 contributions to the D91N minus WT difference in mean squared reference deviation at matching velocity-seed labels. Both segments use the same EEF1A2 core fit. Units are Å^2.

Discussion

The sequence of saved structures locates the first shorter D91N–GDP distance in this preparation. Immediately before minimization the minimum differed by only 0.04 Å between D91N and WT. During minimization the WT minimum increased by 0.93 Å as the closest source-labeled Asp oxygen changed, whereas the D91N minimum changed by less than 0.02 Å. Asp OD1 and OD2 are chemically equivalent carboxylate oxygens. The change in which label ranked first cannot by itself establish a rotamer transition or identify which molecule moved. Later dynamics changed the local geometry in all three D91N runs, including a χ1 transition in seed 47. The opposite sign in the seed-11 static predictions underscores the dependence on construct, starting pose and chemical state.

The first 24 partner residues contributed most of the increase in mean squared reference deviation at seeds 11 and 23. In seed 47 the final 90 residues dominated and the first segment contributed negatively. The fixed EEF1A2 alignment combines relative motion of the partner with its internal rearrangement. The two trans-Asn91 runs also sampled a water-mediated connection to GDP O2B. Seed 47 changed rotamer early and showed no qualifying bridge in the primary window. These occupancies describe how often the geometry was observed at 100 ps sampling. They cannot identify water residence times, stabilization free energies or nucleotide-release rates.

The functional state of the modeled human complex remains unassigned. The two measured docking contacts and the Lys20–Asp91 Cα spacing resemble the four yeast exchange complexes, yet the human Lys224 NZ lies farther from Ser21 OG. The combination is consistent with docking without insertion of the catalytic lysine at the yeast position. None of the four inspected yeast structures shows this combination. An encounter state and a modeling artifact remain possible. WT Asp91 was gauche-minus in the primary window and frequently accepted a hydrogen bond from Thr24. Asp91 was trans in all six inspected crystal copies. A contact to the Lys224 backbone carbonyl also has a different chemical meaning from placement of its terminal NZ. The salt bridge between Asp91 and Lys20 and the hydrogen bond with Ser21 described by Crépin et al. [1] suggest a specific hypothesis. Because Asn91 lacks the carboxylate needed for this salt bridge, we predict a larger D91N effect on EEF1B2-stimulated GDP release than on basal release. Neither rate was measured here.

Human-cell evidence also constrains the interpretation. In a doctoral thesis, McLachlan reported co-immunoprecipitation from transfected HEK293T cells in biological triplicate. The study detected no statistically significant difference between D91N and WT in recovery of eEF1B subunits, whereas D252H showed reduced recovery [9]. With three biological replicates, the assay had limited sensitivity to differences and could not establish equivalence. Relative subunit recovery measures neither binary affinity nor the rate of GDP release. Combined with the yeast abundance observation, this evidence gives particular weight to measuring stimulated release at matched concentrations of active human protein.

Three trajectories per condition sampled velocity and dynamical variation for one predicted scaffold, one preparation per condition, fixed protonation and GDP without Mg. Twenty-five nanoseconds afforded limited sampling of rotamer transitions or slower partner rearrangement. The primary-window core and fragment RMSDs depend on the alignment mask, reference and fragment boundary. The early core contrast may reflect relaxation from the restrained preparation. The final 100 ps of equilibration already had zero positional restraint, so there was no new restraint release at production zero. The time-step and hydrogen-mass-repartitioning sensitivity of solvent geometry remains untested. Static distances were initially selected after inspection, and numerical acceptance criteria were revised after the first WT run. The simulations sampled neither GDP release nor a binding equilibrium. The failed Mg-containing preparation leaves the physiological relevance of the Mg-free state unresolved. One observed D91N χ1 transition is insufficient to estimate equilibrium rotamer preferences.

Conclusions

In a Mg-free human complex built from one WT scaffold, the shorter residue-91–GDP distance in D91N first appeared after minimization, chiefly through an increase in the WT minimum. The distance ordering persisted in all three production-start comparisons and all three primary-window run means. Two D91N runs retained trans Asn91 and sampled a water bridge to GDP. The third changed rotamer before 1 ns. The human model reproduced selected docking contacts while the Lys224 NZ–Ser21 OG run means exceeded the distances in the four yeast exchange complexes. These observations motivate a direct comparison of basal and EEF1B2-stimulated GDP release at matched concentrations of active WT and D91N protein.

Unanswered questions and further experiments

1. How much of the partner displacement reflects internal deformation? The completed segment and per-residue analyses use the original EEF1A2 core alignment. A partner-centered fit, compared with alternative EEF1A2 alignment masks, would help separate motion of the partner relative to EEF1A2 from deformation within EEF1B2. Independent starting structures could test whether the same geometric differences recur.

2. How sensitive is the geometry to the modeled state? A second independently supported starting pose and alternative protonation assignments would test whether the post-minimization distance ordering recurs. A Mg-containing comparison requires an ion–phosphate model that maintains credible local coordination through preparation. More seeds or longer trajectories would address variability within each setup. A controlled comparison of the original and normalized sequence alignments would address the separate question of static prediction sensitivity.

3. Does D91N change stimulated GDP release? Compare GDP release for purified human WT and D91N at matched concentrations of soluble, correctly folded, nucleotide-competent EEF1A2. Measure the basal rate and its response across EEF1B2 concentrations, with controlled nucleotide loading and Mg. Estimate basal release, maximal stimulation and the apparent half-maximal EEF1B2 concentration under the stated assay conditions. That kinetic concentration, often written $K_1/_2$, can depend on multiple reaction steps. Measure binding independently to estimate the equilibrium dissociation constant. Independent protein preparations and an orthogonal measurement of GDP release would help distinguish altered association, altered stimulation and fluorescent-nucleotide effects. An altered basal rate would instead motivate testing intrinsic nucleotide handling. If apparent differences disappear after matching active protein concentration, soluble abundance or folding warrants priority. The experiments are proposals.

Data availability

The companion data package contains the original scalar series, preparation checkpoints, topologies, atom maps, analysis definitions and replay scripts for the nine Mg-free trajectories. Full-system and solute coordinate segments are organized in one archive per trajectory. Separate archives contain the six structural predictions, their sequence alignments, and the measurements and coordinates from the three Mg-containing pilot runs. Supplementary tables and Figure S4 accompany the manuscript. Public crystal coordinates are available from the Protein Data Bank under 4C0S [1], 1F60 [10], 1G7C, 1IJE and 1IJF [2].

Author's study page: https://www.filippogalbo.com/research/eef1a2-d91n/preprint. Please direct requests for the separate research data archives to the corresponding author.

Author statement

The author undertook this research to contribute to the field and to benefit public health.

Funding

The author personally funded this research.

Competing interests

The author declares no competing interests.

Use of AI-assisted tools

The author used Gemini Neon, Claude Fable 5.2, Claude Opus 5.5, Astra 6 and Astra 6.2 to assist with manuscript drafting and editing, analysis-code development and checks against archived measurements.

References

1. Crépin T, Shalak VF, Yaremchuk AD, et al. Mammalian translation elongation factor eEF1A2: X-ray structure and new features of GDP/GTP exchange mechanism in higher eukaryotes. Nucleic Acids Research. 2014, 42, 12939–12948. https://doi.org/10.1093/nar/gku974

2. Andersen GR, et al. Crystal structures of nucleotide exchange intermediates in the eEF1A–eEF1Bα complex. Nature Structural Biology. 2001, 8, 531–534. https://doi.org/10.1038/88598

3. Pittman YR, Valente L, Jeppesen MG, Andersen GR, Patel S, Kinzy TG. Mg^{2+} and a key lysine modulate exchange activity of eukaryotic translation elongation factor 1B alpha. Journal of Biological Chemistry. 2006, 281, 19457–19468. https://doi.org/10.1074/jbc.M601076200

4. Lam WWK, Millichap JJ, Soares DC, et al. Novel de novo EEF1A2 missense mutations causing epilepsy and intellectual disability. Molecular Genetics & Genomic Medicine. 2016, 4, 465–474. https://doi.org/10.1002/mgg3.219

5. Minoia M, Quintana-Cordero J, Jetzinger K, et al. Chp1 is a dedicated chaperone at the ribosome that safeguards eEF1A biogenesis. Nature Communications. 2024, 15, 1382. https://doi.org/10.1038/s41467-024-45645-w

6. Davies FCJ, et al. Recapitulation of the EEF1A2 D252H neurodevelopmental disorder-causing missense mutation in mice reveals a toxic gain of function. Human Molecular Genetics. 2020, 29, 1592–1606. https://doi.org/10.1093/hmg/ddaa042

7. Passaro S, Corso G, Wohlwend J, et al. Boltz-2: Towards Accurate and Efficient Binding Affinity Prediction. bioRxiv preprint. 2025. https://doi.org/10.1101/2025.06.14.659707

8. Eastman P, Galvelis R, Peláez RP, et al. OpenMM 8: Molecular Dynamics Simulation with Machine Learning Potentials. Journal of Physical Chemistry B. 2024, 128, 109–116. https://doi.org/10.1021/acs.jpcb.3c06662

9. McLachlan F. Investigating the role of eukaryotic translation elongation factor eEF1A2 in autism, epilepsy and intellectual disability. PhD thesis, University of Edinburgh, 2020. Chapter 4, section 4.3.2, Figure 4.2. Edinburgh Research Archive. https://doi.org/10.7488/era/75

10. Andersen GR, Pedersen L, Valente L, Chatterjee I, Kinzy TG, Kjeldgaard M, Nyborg J. Structural basis for nucleotide exchange and competition with tRNA in the yeast elongation factor complex eEF1A:eEF1Balpha. Molecular Cell. 2000, 6, 1261–1266. https://doi.org/10.1016/S1097-2765(00)00122-2

11. Jank T, Belyi Y, Wirth C, et al. Protein glutaminylation is a yeast-specific posttranslational modification of elongation factor 1A. Journal of Biological Chemistry. 2017, 292, 16014–16023. https://doi.org/10.1074/jbc.M117.801035

12. Paulet A, Bennett-Ness C, Ageorges F, et al. Expansion of the neurodevelopmental phenotype of individuals with EEF1A2 variants and genotype-phenotype study. European Journal of Human Genetics. 2024, 32, 1144–1149. https://doi.org/10.1038/s41431-024-01560-8

13. Carvill GL, Helbig KL, Myers CT, et al. Damaging de novo missense variants in EEF1A2 lead to a developmental and degenerative epileptic-dyskinetic encephalopathy. Human Mutation. 2020, 41, 1263–1279. https://doi.org/10.1002/humu.24015